Check for updates

Effect of surface energy and roughness on cell adhesion and growth – facile surface modification for enhanced cell culture†

B. Majhy,[a] P. Priyadarshini[a] and A. K. Sen (ID) *[ab]

In vitro, cellular processing on polymeric surfaces is fundamental to the development of biosensors, scaffolds for tissue engineering and transplantation. However, the effect of surface energy and roughness on the cell–surface interaction remains inconclusive, indicating a lack of complete understanding of the phenomenon. Here, we study the effect of surface energy (E_s) and roughness ratio (r) of a polydimethylsiloxane (PDMS) substrate on cell attachment, growth, and proliferation. We considered two different cell lines, HeLa and MDA MB 231, and rough PDMS surfaces of different surface energy in the range $E_s = 21$–100 mJ m^{-2}, corresponding to WCA $161°$–$1°$, and roughness ratio in the range $r = 1.05$–3, corresponding to roughness 5–150 nm. We find that the cell attachment process proceeds through three different stages marked by an increase in the number of attached cells with time (stage I), flattening of cells (stage II), and elongation of cells (III) on the surface. Our study reveals that moderate surface energy ($E_s \approx 70$ mJ m^{-2}) and intermediate roughness ratio ($r \approx 2$) constitute the most favourable conditions for efficient cell adhesion, growth, and proliferation. A theoretical model based on the minimization of the total free energy of the cell–substrate system is presented and is used to predict the spread length of cells that compares well with the corresponding experimental data within 10%. The performance and reusability of the rough PDMS surface of moderate energy and roughness prepared *via* facile surface modification are compared with standard T-25 cell culture plates for cell growth and proliferation, which shows that the proposed surface is an attractive choice for efficient cell culture.

1. Introduction

Recent progress in cell biology, regenerative medicine, and tissue engineering has made an astonishing breakthrough in transplant and tissue repair using artificial regeneration that necessitates several artificial biological systems.[1] Hence, a thorough understanding of controlled cell behaviors, including cell adhesion, growth, differentiation, and migration *in vitro* on an artificial surface, is of great interest to life science and materials research. In nature, cellular behaviors have been mainly controlled by the extracellular matrix (ECM), which provides chemical and structural integrity to the cells and also regulates the metabolism, growth, proliferation, and transport process of cells.[2] The interaction between external surfaces and

[a]Fluid Systems Laboratory, Department of Mechanical Engineering, Indian Institute of Technology Madras, Chennai, India. E-mail: ashis@iitm.ac.in

[b]Micro Nano Bio Fluidics Group, Indian Institute of Technology Madras, Chennai, India

† Electronic supplementary information (ESI) available: The different parameters used for predicting the length of a particular cell for a given surface of certain surface energy and roughness. The experimental images of cell growth and proliferation on normal PDMS surface. The experimental image of cell growth on extremely low surface energy surfaces such as the superhydrophobic surfaces. See DOI: 10.1039/d1ra02402g

cells has been a topic of interest, investigated by considering various artificial polymer surfaces with different chemical, topological, and mechanical cues that control cell behaviors.[3,4]

When a polymeric substrate is in contact with a fluid medium suspending biological cells, the cellar activities such as adsorption of serum protein, cell adherence, cell growth, and proliferation mainly depend on the surface energy of the substrate. The relationship between cellular behaviors and the surface energy of polymer surfaces has been investigated in literature.[5–11] Studies have suggested that, in general, cells prefer to grow on higher energy surfaces irrespective of whether the polymer substrate is functionalized with or without proteins. Specifically, the polar groups on polymer surfaces interact with cell surface groups and create chemical bonds, whereas non-polar groups create non-specific short-range interactions such as van der Waals interaction. On the contrary, some studies have demonstrated preferential cell growth on low-energy surfaces such as superhydrophobic surfaces.[12,13] Besides chemical influence, surface topographical factors such as roughness[14–16] and porosity[17] of polymer surfaces can also significantly influence cell–substrate interactions. Experimental studies have shown that surface micro/nano topography could be as unimportant as chemical interactions in modulating cellular behaviors.[18] Most mammalian adherent

cells must adhere to a surface during culture for their survival and the rough structures on a surface promote mechanical anchoring to the cells.[19] Surface topography can also significantly affect the protein adsorption into substrates and, therefore, control the response of cells towards the surfaces. A few studies have reported contrasting observations – the suppression of cell adhesion, growth, and proliferation with an increase in surface micro/nano roughness.[20] Further, another study has demonstrated that surface roughness has a minor influence on cellular behavior.[21]

A review of the literature reveals contrasting observations about the effect of surface energy and roughness on the cell–surface interaction, indicating a lack of complete understanding of the phenomenon. Further, most of the studies have focused on the effect of surface roughness or wettability on cell–surface interaction and their combined effect is rarely investigated.[18,22] Clearly, conclusive studies on the role of surface energy and roughness in cell–surface interaction are missing in the literature. Here, we study the combined effect of surface energy and roughness on cellular behavior such as attachment, growth, and proliferation. We take two different cell lines, cervical cancer cell line, HeLa, and breast cancer cell line, MDA MB 231, and vary wettability and roughness of a polydimethylsiloxane (PDMS) surface – from complete wetting (*i.e.* superhydrophilic) with water contact angle (WCA) $\sim 0°$ to complete non-wetting (*i.e.* superhydrophobic) with WCA $\sim 165°$, and surface roughness in the range 5 to 150 nm. We explain the mechanism of cell adhesion and study the effect of surface energy and roughness on cell adhesion, growth, and proliferation in terms of cell length and multiplication. Suppression of cell–surface interaction on extreme wetting and rough surfaces is also explained. A theoretical model is used to predict the size of attached cells on different surfaces with varying wettability and roughness. A comparison of the cell growth and proliferation on the rough PDMS surface prepared *via* facile surface modification with the standard cell culture plate is also presented.

2. Materials and methods

2.1 Cell sample preparation

The cell lines purchased from National Centre for Cell Sciences, Pune, India, and stored at $-80\,°C$ in the deep freezer (Thermo Fisher Scientific, USA) are revived at $37\,°C$. The cells are seeded into a T-25 flask with Dulbecco's Modified Eagle Medium (DMEM) (Himedia, India) and incubated in a CO_2 incubator (Thermo Fisher Scientific, USA) at $37\,°C$, 5% CO_2 level and >95% relative humidity for culture. The DMEM contains an antibiotic mix of 62.77 mg penicillin, 100 mg streptomycin, and 50 mg gentamicin, and 20% fetal bovine serum. When the cells are fully grown and proliferated, the DMEM is removed, and the attached cells are washed with Phosphate Buffered Saline (PBS). Then, for breaking the bonds between the cells and surface and detachment, cells are trypsinized with $1\times$ trypsin and then incubated in a CO_2 incubator for 3 min. Then, 1 mL of fresh DMEM is added to the detached cells and centrifuged (Remi, India) at 1800 rpm for 5 min. Finally, after removing the

supernatant, 1 mL fresh media is added to the pellet, and the cells are gently resuspended for further use.

2.2 Fabrication of surfaces of different wettability and roughness

First, polydimethylsiloxane (PDMS) and its curing agent (Sylgard 184, Dow Corning, U.S.A.) at a ratio of 5 : 1, and 10% of *n*-hexane are thoroughly mixed. The mixture is left in the air for 30 min for degassing. Then, clean glass slides (Blue Star, Sigma-Aldrich) are coated with the above mixture using a spin coater at 4000 rpm for 10 s. The PDMS-coated glass substrate is partially cured on a hot plate at $85\,°C$ for 10 min. The top surface of the partially cured PDMS coating is then brought over a candle flame and moved back and forth at a constant velocity in the horizontal plane for 0–2 min, for growing a uniform layer of carbon soot particles. Since the PDMS coating is already partially cured, although the soot particles penetrate the coating, they do not strongly adhere to the surface. Next, the carbon soot-coated PDMS surface is exposed to a high-speed water jet to wash away the loosely bonded soot particles from the surface. The removal of soot particles produces a superhydrophobic (SHB) PDMS surface, whose roughness is controlled in the range of 5–150 nm depending on sooting time and location across the flame.[23] The water contact angle (WCA) of the surfaces is measured using a goniometer (DSA25, KRÜSS GmbH) and the roughness of different surfaces is measured using a stylus-based profilometer (Bruker, U.S.A.). The WCA on smooth PDMS and rough PDMS surfaces with 4 s and 10 s sooting time respectively are shown in Fig. 1a. The profilometry results for a smooth PDMS surface and rough PDMS surfaces are presented in Fig. 1b. While a smooth PDMS surface is hydrophobic with a WCA $\sim 110°$ and has low surface energy, E_s ~ 21 mJ m^{-2}, the WCA increases due to the addition of nano-scale roughness.[24]

The surface energy of the rough surfaces is measured by goniometer using the OWRK method, which is given as $\frac{E_L(\cos\ \theta + 1)}{2(E_L^D)^{1/2}} = (E_S^P)^{1/2}\left[\frac{(E_L^P)^{1/2}}{(E_L^D)^{1/2}}\right] + (E_S^D)^{1/2}$, together with the Cassie–Baxter relation $\cos\theta_{C-B} = f(r\cos\theta + 1) - 1$. Here, $E_s = E_S^P + E_S^D$, where E_S^P and E_S^D are the solid surface energies due to the polar component and disperse component, respectively, E_L^P and E_L^D are the liquid surface energies due to the polar component and disperse component, respectively and diiodomethane is used as the non-polar liquid and water as polar liquid. For example, for a surface having a WCA $\theta_{C-B} \approx 8°$, solid fraction $f \approx 0.15$ and roughness ratio $r \approx 2$, total solid surface energy is 70 mJ m^{-2} which is a combination of $E_S^P = 36$ mJ m^{-2} due to the polar component and $E_S^D = 34$ mJ m^{-2} due to the dispersion component. To obtain high energy rough surfaces of varying WCA and E_s, the SHB surfaces are exposed to oxygen plasma (PDC-002, Harrick Plasma, USA) at a power in the range of 12–30 W and for 30 s to 2 min. Upon exposure to oxygen plasma, the non-polar groups (*i.e.* CH_3 groups) of the hydrophobic and superhydrophobic PDMS surface change to high energy polar groups resulting in hydrophilic and superhydrophilic (SHL) surfaces (Fig. 1a).[23] The increase in surface
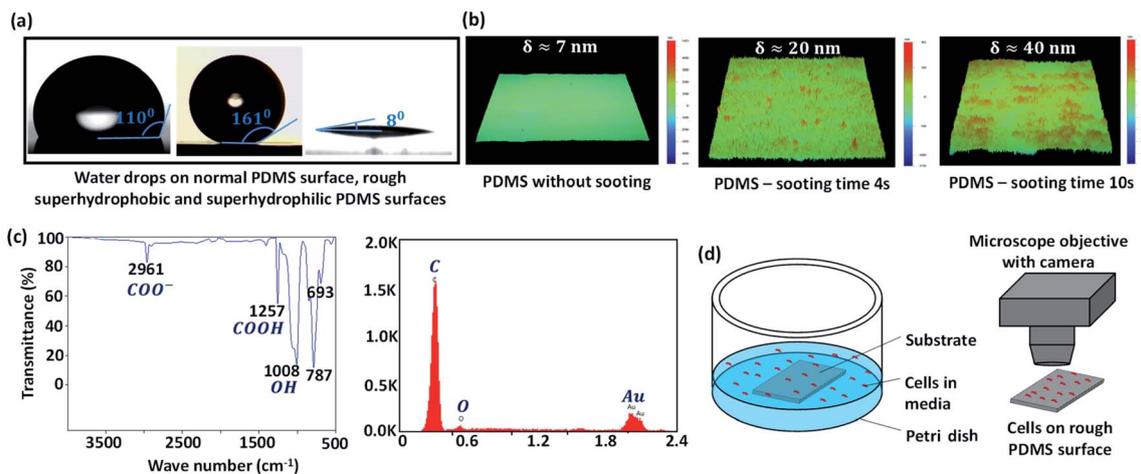
Fig. 1 (a) Experimental images of water drops on normal PDMS surface, rough superhydrophobic and superhydrophilic PDMS surfaces, (b) profilometry results for a smooth PDMS surface and rough PDMS surfaces with a sooting time of 4 s and 10 s, (c) FTIR and EDAX results for the superhydrophilic (high energy) rough PDMS surface, (d) schematic of the experimental setup used for studying cell attachment, growth, and proliferation on rough PDMS surfaces.

Table 1 FTIR band assignment

Wavenumber (cm^{-1})	Assignment
787	–C–C stretch
1008	–OH bend
1128	–C–O– stretch
1257	–C=O bend
1370	–CH– deformation including symmetric and asymmetric bend
1750	–C=O carbonyl stretch
2961	–CH– stretch

energy is primarily due to an increase in the polar component, whereas the dispersed component remains unchanged. The increase in surface energy is mainly due to the polarized ions, carboxyl (COOH), carboxylate (COO^-) and hydroxyl (OH) formed on the surface molecules due to the oxygen plasma exposure, which can be observed in the Fourier-transform infrared spectroscopy (FTIR) and Energy-dispersive X-ray spectroscopy (EDAX) results in Fig. 1c and Table 1. The WCA and E_s of the rough PDMS surfaces having different roughness values used in the present study are presented in Table 2.

2.3 Cell culture

To culture cells on the rough PDMS surfaces, a 5 cm diameter Petri dish and 2×2 cm^2 rough PDMS surface is thoroughly sterilized using 70% ethanol spray and then under the UV light for 30 min; the surface is placed in the Petri dish (Fig. 1d). Each of the two cell lines, at a concentration of $\sim 2 \times 10^5$ mL^{-1} is seeded, and the Petri dish is covered with an ethanol-cleaned glass slide leaving a small air gap. Then the setup is gently placed inside the CO_2 incubator. To monitor cell attachment, growth, and proliferation, the images of the cells on the surface is captured after 24, 48, and 72 h under an inverted microscope

(IX 73 Olympus, Japan) with 5X-60× objective lenses and a high-resolution camera (FASTCAM SA5, Photron, UK) (Fig. 1d). To monitor the initial progress in cell attachment, the images of the cells are also captured for the first 30 min. The length of the cells at different surface energy and roughness are measured to characterize the cell attachment and growth. The number of cells is counted at different time points using Image J software to quantify cellular proliferation.

3. Results and discussion

3.1 Various stages of cell growth and proliferation

We first study the attachment of HeLa cells seeded into a Petri dish containing a rough PDMS surface of $E_s \approx 70$ mJ m^{-2} and roughness ratio $r \approx 2$, at different time points, as shown in Fig. 2a. It is observed that the number of attached cells increases rapidly with time up to $t = 15$ min, after which the number of attached cells remains constant (see Fig. 2b). The cells remain spherical up to $t = 15$ min (see inset of Fig. 2a), and after 15 min they start to lose sphericity suggesting the onset of cell attachment with the surface and cells begin to flatten (see

Table 2 Roughness (δ), and roughness ratio (r) contact angle (°), surface energy (E_s), of the different rough PDMS surfaces used in the present study

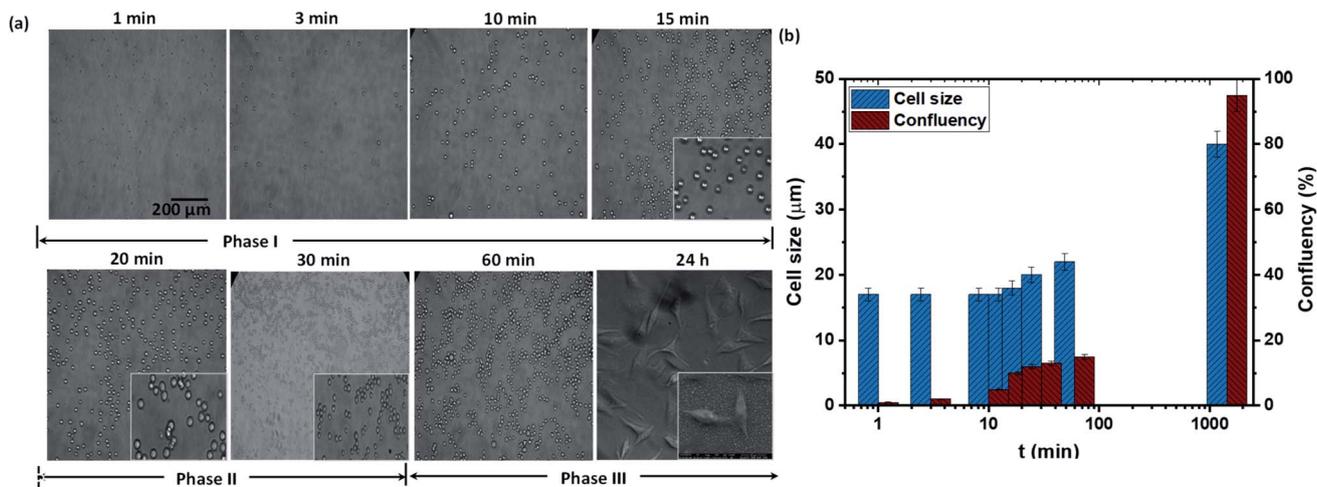| Sl. no.	Roughness ratio, r	Roughness, δ (nm)	Contact angle θ (°)	Surface energy, E_s (mN m^{-1})
1	2	~30	40 ± 1	55
2		~30	30 ± 1	60
3		~30	1 ± 1	80
4		~30	8 ± 1	70
5	2.20	~40	8 ± 1	
6	1.50	~20	8 ± 1	
7	1.05	~7	8 ± 1	

Fig. 2 (a) Attachment of HeLa cells seeded into a Petri dish containing a PDMS rough surface of $E_s \approx 70$ mJ m^{-2} and roughness ratio $r \approx 2$, at different time points, (b) variation of the number of cells attached to the surface and length of the cells attached to the surfaces with time.

inset of Fig. 2a at $t = 20$ min). A rapid increase in cell length is observed beyond $t = 60$ min, which indicates the spreading of cells on the surface (see Fig. 2b). Typically, the cell adhesion process occurs in three major stages: stages I, II, and III. A detailed schematic illustration of cell–substrate interaction from a non-adherent state to the stage of cytoskeleton organization in stable adhesion is depicted in Fig. 3. When a cell comes in contact with a surface, first, the cell membrane passively adheres to the surface through a combination of short-

ranged physicochemical interactions attributed to the van der Waals forces, steric and coulombic forces,[4] which can be referred to as phase I and observed for $t < 15$ min. In phase II, the functional groups such as hydroxyl (OH) and carboxyl (COOH) present on the mild superhydrophilic surface control essential protein adsorption from the cell surface onto the substrate surface for creating integrin bonding with cell ligands,[9] and as a result, the cell starts to spread, which is observed for $t = 15$–60 min. Although there are no specific
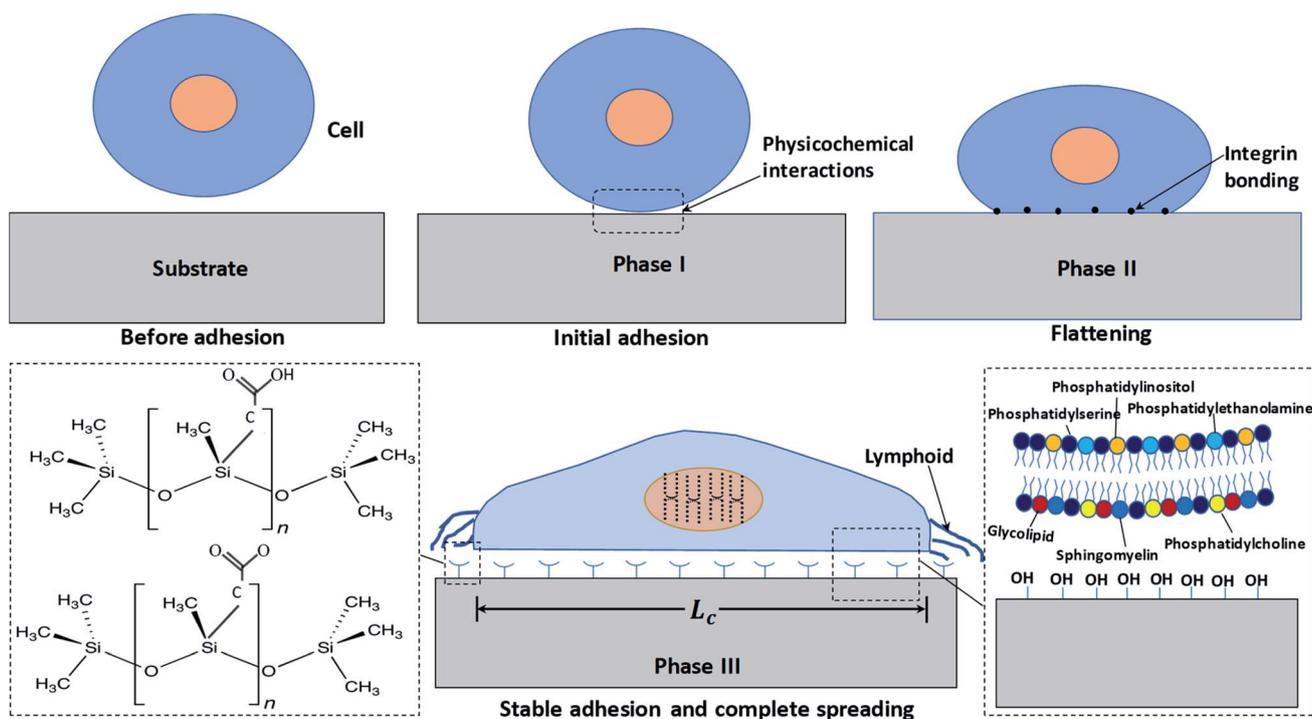

Fig. 3 A detailed schematic illustration of cell–substrate interaction from a non-adherent state to the stage of cytoskeleton organization in stable adhesion. The extended view on the bottom right shows the cell membrane's surface chemistry, whereas the extended view on the bottom left shows the substrate surface chemistry.

receptor molecules are placed in the substrate, whereas the surface functional groups like hydroxyl (OH) and carboxyl (COOH) control essential protein adsorption on the mild superhydrophilic surface for creating integrin bonding with cell ligands.[9] Finally, in phase III, there is an organization of cytoskeleton to form focal adhesions with the help of lymphoid coming out of the cell membrane that leads to complete spreading of the cell (see the SEM image in Fig. 2a, at $t = 24$ h).

3.2 Theoretical model for the estimation of spread length of a cell

The spread length of a cell on a surface can be determined by minimizing the total free energy of the cell–substrate system. The total energy is the net effect of the surface energy E_s, which drives cell adhesion and elongation, and the energy needed for recruiting new adhesive molecules, and the elastic energy, which opposes adhesion and elongation of the cell membrane. Here we minimize the total energy with respect to cell size for finding out the critical size of a cell for a particular system having certain values of surface energy and roughness. By considering the surface energies and volumetric elastic energy, the expression for total Gibb's free energy is obtained as follows,

$$G = r(E_{sc} - E_s)\frac{WL_c}{2} + \frac{1}{2}KV_c\varepsilon^2 \qquad (1)$$

where E_{sc} is interfacial energy between cell and substrate, E_s is the surface energy of the substrate at the solid–air interface and r is the roughness ratio of the substrate, which is defined as the ratio between the actual and projected solid surface area, W and L_c are maximum width and length of the cell respectively. Here, K, V_c and ε are the elastic modulus, volume, and strain of the cell, respectively.

The interfacial energy E_{sc} due to ligand–receptor binding between a cell and a substrate can be estimated as,[14]

$$E_{sc} = \rho_b\mu_b - \rho_r\mu_r \qquad (2)$$

where ρ_b is the density of ligand–receptor binding, and $\mu_b = \mu_b^0 + k_BT\log(\rho_b)$ is the chemical potential of a ligand–receptor bond, ρ_r is the density of free receptor molecules, $\mu_r = \mu_r^0 + k_BT\log(\rho_r)$ is the chemical potential of a free receptor (μ_b^0 and μ_r^0 are the standard state chemical potentials of ligand–receptor bond and free receptor respectively), k_B is Boltzmann constant and T is temperature. Therefore, we get

$$E_{sc} = \left[-\left(\frac{\mu_r^0 - \mu_b^0}{k_BT}\right) + \log\left(\frac{\rho_b}{\rho_r}\right)\right]k_BT \qquad (3)$$

By minimizing the total Gibb's free energy with respect to the length of the cell (L_c), i.e. employing $(dG/dL_c) = 0$, the size of the cell is estimated as

$$\frac{rw}{2}(E_{sc} - E_s) + \frac{KV}{L_{c_0}^2}\Delta L_c = 0 \qquad (4)$$

where L_{c_0} and ΔL_c are the initial length and change in length of the cell, respectively. The above equation suggests that the

spread length of a cell is a function of both roughness ratio and surface energy. The different parameters used for predicting the length of a particular cell for given surface energy and roughness are presented in Table S1.† For the conditions used in Fig. 2a, the length of the cell in its complete spreading condition is predicted to be 40 μm from eqn (4), which compared well with the measured value of 41 ± 1 μm (see SEM image in Fig. 2a) within 10%. Further, we use the model to predict the length of the cells on surfaces of different surface energy and roughness, which is discussed next.

3.3. Effect of surface energy and roughness on cell growth and proliferation

The cell–substrate interaction mainly depends on ligand molecules on the surface of a cell, secretion of proteins, and the polar and non-polar groups present on a surface. Unfortunately, we have no control over molecules over the surface of a cell, or at least it is not trivial, but it is possible to actively control the molecules on a substrate, which will govern specific ligand–receptor bonds and non-specific short-ranged van der Waals and electrostatic interactions and therefore the cell–surface interaction. As surface molecules or surface chemistry decide the surface energy of a substrate, hence surface energy plays a prominent role in cell adhesion, growth, and proliferation. Mechanical stability of cells during growth and quantitative interaction of cells with surface molecules is decided by the area of contact between cell and substrate that depends on the surface topological factors such as roughness, and therefore surface roughness also has a vital role in cell adhesion, growth, and proliferation.

Effect of surface energy. We study the effect of surface energy (E_s) on the cell attachment, growth, and proliferation by taking the HeLa and MDA MB 231 cell lines of average cell size of 17 μm and 15 μm respectively, and PDMS surface of a fixed roughness, $\delta \approx 30$ nm with roughness parameter $r = 2$, and varying surface energy in the range $E_s = 21$–100 mJ m^{-2}, as presented in Table 1. The PDMS substrates of different surface energy are seeded with the two cell types separately, and cell behavior is monitored at different time points, as described in the materials and methods section. The two different cell lines, HeLa and MDA MB 231 were chosen because of their distinct elastic modulus (K) values: for HeLa and MDA MB 231, $K = 763 \pm 93$ Pa and $K = 182 \pm 34.74$ Pa, respectively.[25] PDMS is used as the substrate material due to its attractive properties such as biocompatibility, easy wettability control, inert and low cost.[26] The elasticity of a substrate can also influence cellular behaviour, as cells have the ability to sense the mechanical properties of a substrate in contact by applying a force and respond to the substrate by organizing the cytoskeleton and adjusting the overall structure.[27,28] In the present case, PDMS is used as the substrate material whose stiffness can be modulated by adjusting the base-to-crosslinker ratio.[29] It was found that stiffer PDMS substrates significantly promote cell spreading and consequently cell culturing,[30,31] and therefore, we have used a stiffer PDMS surface having stiffness $K = 1000$ kPa in the present study.

The experimental images of the HeLa and MDA MB 231 cells cultured on surfaces of different surface energy at 24 h, and the variation of the spread length of the cells (cell growth) and the number of cells (cell proliferation) are presented in Fig. 4a–c. For HeLa cells, we observe that cell growth and proliferation is enhanced with an increase in surface energy (*i.e.* enhanced surface polar groups), up to a critical surface energy of $E_s \sim 70$ mJ m^{-2}. For example, it is seen that for HeLa cells, the cell length and confluency respectively increases from 17 µm and ~10% at surface energy 21 mJ m^{-2} to ~40 µm and ~95% at surface energy of 70 mJ m^{-2}. The enhancement in cell growth and proliferation can be attributed to the cellular–surface interactions that are predominantly controlled by integrins present on the plasma membrane and surface polar groups and non-polar groups (see Fig. 3). Cell membrane mainly consists of a liquid bilayer of lipid, embedded proteins, and water. The lipid bilayer contains phospholipids (see Fig. 3), which are amphipathic molecules, with phosphate-rich hydrophilic heads on the outside and hydrophobic tails on the inside. The cell membrane is similar to a charged object suspended in a mixture of dissolved ions, and the increase in surface energy corresponds to the increase in the density of surface polar groups (see Fig. 1c). Thus, adhesion, growth, and proliferation are promoted with an increase in surface energy because the hydroxyl and carboxyl groups present on the surface (see Fig. 1c) could potentially form hydrogen bonds with cell surface lipids and ions. However, above critical surface energy, cell growth and proliferation decrease, which can be attributed to a stronger adhesion to the surface, possibly hindering the freedom of integrins to modulate. Therefore, after a certain energy level, the cell growth rate, and consequently the proliferation is suppressed. The theoretical model (see eqn (4)) is used to predict the spread cell length, which shows a good

agreement with the experimental measurements within 10% (Fig. 4c). The results show that the maximum cells growth and proliferation for MDA MB 231 cell line are observed at relatively lower surface energy, $E_s = 65$ mJ m^{-2} (see Fig. 4b and c), compared to $E_s = 70$ mJ m^{-2} for the HeLa cells, which can be attributed to higher deformability [25] and consequently enhanced spreading of the MDA MB 231 cells compared to the HeLa cells.

Cells are cultured on normal PDMS surfaces (only with the inherent roughness and without added roughness due to candle-sooting) of different surface energy. The surfaces are fabricated by coating a layer of PDMS at 5 : 1 with 10% *n*-hexane on a glass slide, followed by thermal curing on a hot plate at 85 °C for 10 min without candle sooting, which resulted in an inherent roughness, $\delta \approx 5$ nm or a roughness ratio, $r = 1.05$. The surface energy of the substrate is varied in the range $E_s = 21$–100 mJ m^{-2} by exposing the surface to oxygen plasma. Similar to the nanostructured rough surfaces, we observed an increase in cell growth and proliferation with an increase in the surface energy up to a critical surface energy of 75 mJ m^{-2}, and then cell growth and proliferation decrease with a further increase in surface energy (see Fig. S1†). But in comparison to a rough surface, the cell growth and proliferation on the smooth surface are observed to have been suppressed, which highlights the role of roughness on the cell behavior. Further, on culturing cells on extremely low surface energy surfaces such as the superhydrophobic surfaces having energy $E_s \approx 21$ mJ m^{-2} and with varying roughness ratio of $r \approx$ 1.1–2.75, we observe that dead agglomerated cells floating in the media fluid (see Fig. S2†), which is possible because the surface energy is not adequate for promoting cell adhesion and adsorption of different proteins on the cell membrane to the substrate.
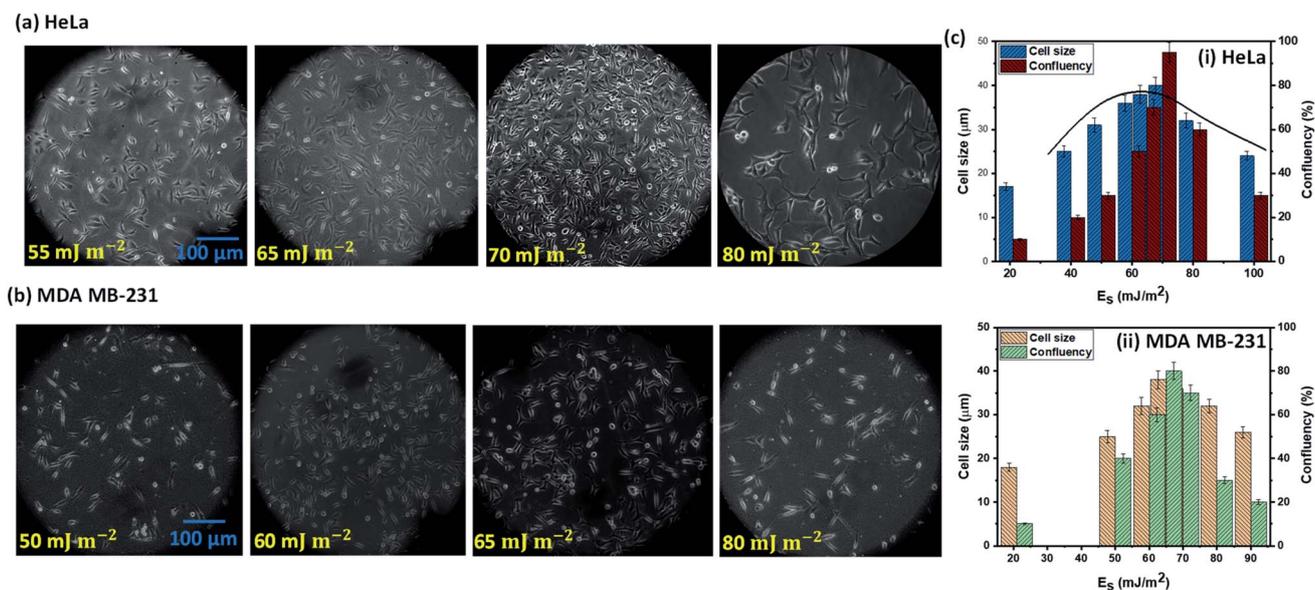

Fig. 4 The experimental images of (a) HeLa and (b) MDA MB 231 cells cultured on surfaces of different surface energy at 24 h, (c) the variation of the spread length of the cells (cell growth), and the number of cells (cell proliferation) with surface energy, surface roughness ratio $r = 2$ in all the cases.

Effect of roughness. Next, we study the effect of surface roughness on cell growth and proliferation by taking PDMS surfaces having a fixed surface energy of $E_s = 70$ mJ m^{-2} and varying its roughness in the range $\delta \approx 5$–150 nm with roughness parameter $r = 1.05$–3. HeLa and MDA MB 231 cells are seeded into the Petri dish containing the PDMS substrates of different roughness and the cell growth and proliferation are monitored at different time points, as described in the materials and methods section. As the elastic modulus of the cells is small, *i.e.* $K = 763 \pm 93$ Pa for HeLa and $K = 182 \pm 34.74$ Pa for MDA MB-231, a cell can be treated as a soft elastic body resting on a rigid rough surface. Thus, the cell membrane penetrates into the grooves of the rough structure to minimize the surface energy of the cell–substrate system. Such behavior of a cell is similar to the invasion of a liquid drop into a rough surface [25], exhibiting Wenzel and Cassie–Baxter approximations. As the cell membrane penetrates into the grooves of rough structures, all topological factors such as height, width, and spatial distribution of micro/nano roughness affect the cell attachment, growth, and proliferation. Therefore, as compared to the surface roughness which is a topological factor, the roughness ratio r, which is the ratio of actual contact area to the projected area parallel to the plane of a surface is a better controlling parameter for characterizing the cell behavior.

The experimental images of the HeLa and MDA MB 231 cells cultured on surfaces of different roughness at 24 h, and the variation of the spread length of the cells (cell growth) and the number of cells (cell proliferation) are presented in Fig. 5a–d. For both cell lines, we observe that the cell growth

and proliferation increase with an increase in the roughness ratio up to a critical roughness of $r = 2$, beyond which the cell growth and proliferation decrease with further increase in roughness ratio. At low roughness ratios $r < 1.5$, elongation of the cell membrane into the rough grooves is limited (see Fig. 5d) and hence the effective surface area for mechanical attachment of cells is significantly less. As attachment is essential for important cellular processes such as cell migration, cell division, cell–cell interaction, contact inhibition, and apoptosis, and hence the cell growth and proliferation are limited (see Fig. 5c). On increasing the roughness ratio $r = 1.5$–2, the cell wall completely penetrates the grooves in order to minimize the total energy by satisfying the Wenzel state (see Fig. 5d). As a result, maximum cell–substrate interaction takes place in this range of r, which gives rise to stable adhesion, and consequently, the highest cell growth and proliferation (see Fig. 5c). For these intermediate values of r, the effective roughness is appropriate for the formation of integrin clusters that stimulate the formation of focal adhesion points, which are essential for healthy cellular functioning. For high roughness ratio, $r > 2$, the elastic energy of a cell hinders its penetration into surface grooves by satisfying Cassie–Baxter state wherein cells sit over the tips of the rough structures leading to only point-contact with the cell (see Fig. 5d) that significantly reduces cell–substrate interaction causing a drastic drop in cell growth and proliferation (see Fig. 5c). The results show that the maximum cells growth and proliferation for MDA MB 231 cell line are observed at a relatively higher roughness ratio, $r = 2.2$–2.4 (see Fig. 5b and c), compared to r
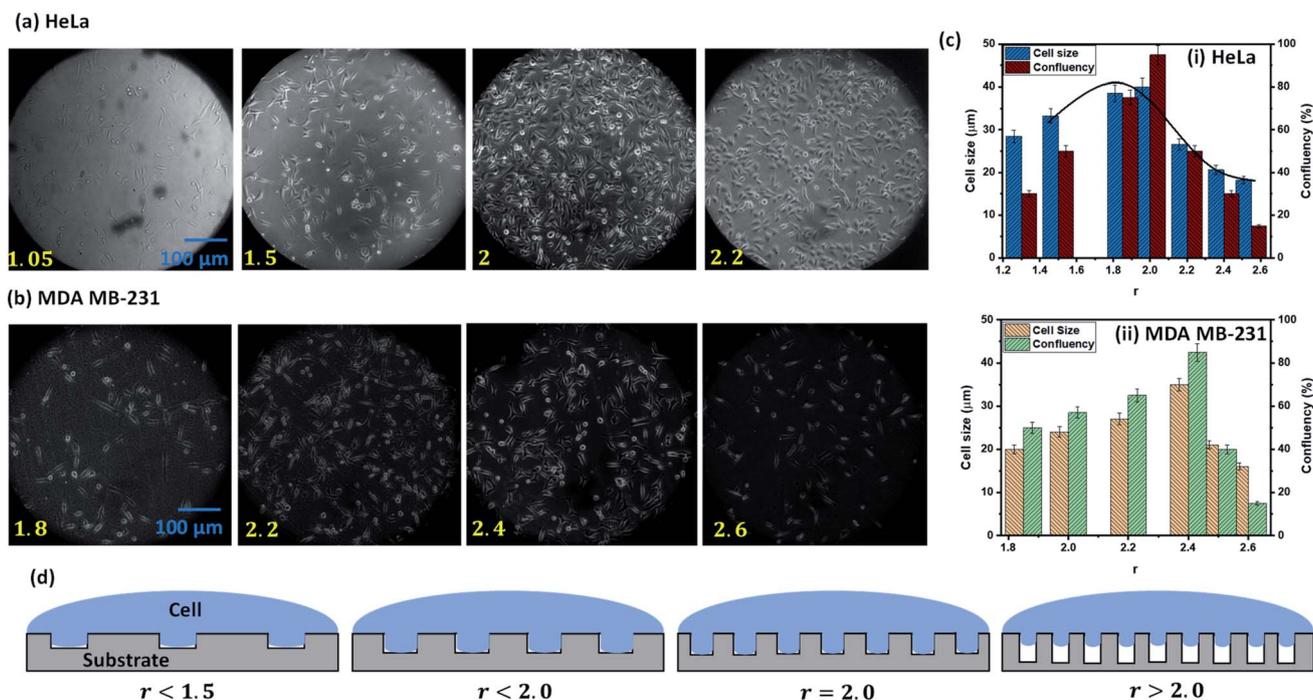

Fig. 5 The experimental images of the (a) HeLa and (b) MDA MB 231 cells cultured on surfaces of different roughness at 24 h, (c) the variation of the spread length of the cells (cell growth), and the number of cells (cell proliferation) with roughness ratio. Surface energy is kept fixed at $E_s = 70$ mJ m^{-2}, (d) schematic illustration of cells resting on surfaces of different roughness ratios.

= 1.9–2 for the HeLa cells, which can be attributed to higher deformability [25] of the MDA MB 231 cells compared to the HeLa cells that allow it to enter into the rough grooves even at a higher roughness ratio with a smaller void between the nanostructures.

In summary, for a moderately rough surface, stable cell adhesion, cell growth, and, consequently, proliferation would be energetically favourable. Surface nano roughness affects protein adsorption and gives contact guidance to the adhered cells to grow. We observed the highest cell growth and proliferation on rough PDMS surfaces for HeLa cells having a surface energy $E_s \sim 70$ mJ m^{-2}, and roughness ratio $r \sim 2$, whereas for MDA MB 231, optimum behaviour observed for $E_s \sim 65$ mJ m^{-2} and $r \sim 2.4$, suggesting moderate wettability and roughness as the preferred condition for cell growth and proliferation. In contrast, superhydrophilic (contact angle < 2°) and superhydrophobic (contact angle > 150°) polymer surfaces are not favorable for cell attachment and growth. Since most cells are hydrophilic or superhydrophilic (for example, the surface energy of HeLa cells is 0.13–0.9 mN m^{-1} (ref. 32)), they tend to spread on a high-energy surface due to the energy gradient between cells surface and substrate, and the roughness enhances the spreading. However, the degree of spreading will also depend on the type of cell–surface combination, which perhaps explains why some cells prefer to spread on superhydrophobic, low-energy surfaces. Thus, those cells whose surface energy is lower or comparable with that of a superhydrophobic substrate will prefer to grow on the superhydrophobic surface.

3.4 Comparison with conventional cell culture plates

One of the limitations of the existing cell culture plates is the reusability issue. We compared the cell attachment, growth, and proliferation behavior of the rough PDMS surface, having a surface energy 70 mJ m^{-2} and roughness ratio $r = 2$, with that on a conventional cell culture plate, T-25 flasks, in terms of reusability. After each cycle of culture, the surfaces were trypsinized and washed thoroughly with PBS. We have used the cells from a fixed batch of cultured cells on both surfaces to avoid any possibility of the effect of a batch-to-batch variation of cells. Experimental images of HeLa cells culture in the T-25 flask over two culture cycles and the rough PDMS surface over three culture cycles are presented in Fig. 6a(i) and b(i), respectively. In the case of the T-25 flask, we observed that the cell growth and proliferation significantly affected even in the second culture cycle, as shown in Fig. 6a(i) and a(ii). This can be attributed to the chemical modification and degradation of the surface of the flask after first seeding. Interestingly on the rough PDMS surface, we observed normal cell growth and proliferation up to the third cycle (see Fig. 6b(i)) with only a marginal (<5%) reduction in confluency, as shown in Fig. 6b(ii). The improved performance of the rough PDMS surface can be attributed to the chemical stability of the surface polar groups, COOH, COO$^-$, and OH, under polar liquids such as water as well as good mechanical stability of the surface, as the surface can withstand a water jet velocity of $\sim$4 m s^{-1} without any surface roughness degradation. The rough PDMS surface can be maintained superhydrophilic for several weeks by dipping it in DI water.[23] As the media DMEM contains mostly water, the surface does not
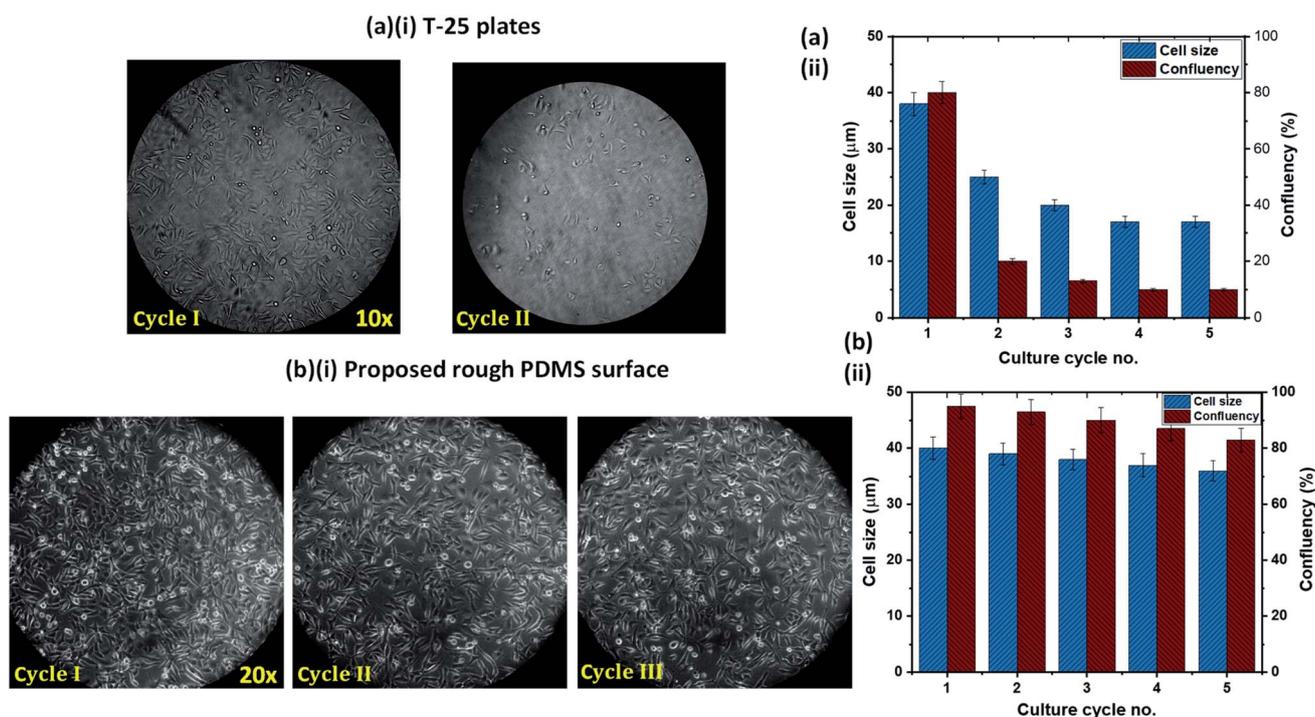

Fig. 6 HeLa cells culture (a)(i) in the T-25 flask over two culture cycles and (a)(ii) corresponding variation of cell length and proliferation over the number of culture cycles. HeLa cells culture (b)(i) on the rough PDMS surface over three culture cycles and (b)(ii) corresponding variation of cell length and proliferation over the number of culture cycles.

degrade and hence can be reused multiple times. Further, we also compared the confluency achieved on both the surfaces in the first seeding cycle, and we observed better confluency in the case of the rough PDMS surface than the standard T-25 culture plate, as shown in Fig. 6a(ii) and b(ii).

4. Conclusions

We studied the cellular behavior of HeLa and MDA MB 231 cells on a rough PDMS surface having surface energy in the range, $E_s = 21$–100 mJ m^{-2}, and roughness ratio in the range $r = 1.05$–3. We found that the cell attachment process occurs in three different stages: in phase I, there is an increase in the number of attached cells with time; in phase II, the cells tend to flatten on the surface and become aspherical, and in phase II, cells spread on the surface. Our study reveals that moderate surface energy ($E_{HeLa} \approx 70$ mJ m^{-2} or $E_{MDA\ MB231} \approx 65$ mJ m^{-2}) and intermediate roughness ratio ($r_{HeLa} \approx 2$ or $r_{MDA\ MB231} \approx 2.4$) give rise to the most favourable conditions for efficient cell adhesion, growth, and proliferation. Higher surface energy leads to the formation of much stronger cell–ligand bonds, thereby leads to enhanced growth and proliferation, but above the critical surface energy, cell growth and proliferation are found to degrade, as a stronger adhesion hinders the liberty of integrins to modulate. Similarly, a higher roughness ratio stimulates the formation of focal adhesion points, which are essential for healthy cellular functioning, and as a result, maximum cell–substrate interaction takes place giving rise to stable adhesion, and consequently, the highest cell growth and proliferation. Above a critical roughness ratio, the elastic energy of the cell hinders the penetration of the cells into surface grooves, where cells sit over the tips of the rough structures leading to only point-contact that reduces cell–substrate interaction drastically which causes a marked drop in cell growth and proliferation. We found that the cell growth and proliferation on rough PDMS surfaces having moderate surface energy ($E_s \approx 70$ mJ m^{-2}) and roughness ($r \approx 2$) is significantly better compared to normal PDMS surfaces ($E_s \approx 70$ mJ m^{-2}) of inherent roughness ($r \approx 1.05$). Cell growth and proliferation were found to be drastically reduced, and even dead cells were found on extreme wetting surfaces, such as superhydrophilic and superhydrophobic surfaces. The theoretical model based on the minimization of the total free energy of the cell–substrate system could predict the spread length of a cell accurately, within 10%. The cell growth and proliferation and reusability of the rough PDMS surface of moderate energy and roughness prepared *via* facile surface modification are compared with T-25 cell culture plates. The results showed comparatively better performance in terms of cell growth and proliferation and reusability of the rough PDMS surface compared to the standard culture plates. The rough PDMS surface thus prepared could be considered as an attractive alternative to standard culture plates for cell culture applications.

Conflicts of interest

There are no conflicts to declare.

Acknowledgements

References

1 C. M. Niemeyer, *Nanobiotechnology*, 2006, **9**, 19–51.
2 D. H. Kim, P. P. Provenzano, C. L. Smith and A. Levchenko, *J. Cell Biol.*, 2012, **197**, 351–360.
3 N. M. Alves, I. Pashkuleva, R. L. Reis and J. F. Mano, *Small*, 2010, **6**, 2208–2220.
4 L. Chen, C. Yan and Z. Zheng, *Mater. Today*, 2018, **21**, 38–59.
5 J. Y. Lim, M. C. Shaughnessy, Z. Zhou, H. Noh, E. A. Vogler and H. J. Donahue, *Biomaterials*, 2008, **29**, 1776–1784.
6 R. Iwata, P. Suk-In, V. P. Hoven, A. Takahara, K. Akiyoshi and Y. Iwasaki, *Biomacromolecules*, 2004, **5**, 2308–2314.
7 W. Feng, S. Zhu, K. Ishihara and J. L. Brash, *Langmuir*, 2005, **21**, 5980–5987.
8 Y. Inoue, T. Nakanishi and K. Ishihara, *Langmuir*, 2013, **29**, 10752–10758.
9 Y. Arima and H. Iwata, *Biomaterials*, 2007, **28**, 3074–3082.
10 C. Pinese, S. Jebors, P. E. Stoebner, V. Humblot, P. Verdié, L. Causse, X. Garric, H. Taillades, J. Martinez, A. Mehdi and G. Subra, *Mater. Today Chem.*, 2017, **4**, 73–83.
11 M. Li, M. J. Mondrinos, X. Chen, M. R. Gandhi, F. K. Ko and P. I. Lelkes, *J. Biomed. Mater. Res., Part A*, 2006, **79**, 963–973.
12 S. C. Luo, S. S. Liour and H. H. Yu, *Chem. Commun.*, 2010, **46**, 4731–4733.
13 S. M. Oliveira, W. Song, N. M. Alves and J. F. Mano, *Soft Matter*, 2011, **7**, 8932–8941.
14 P. Decuzzi and M. Ferrari, *Biomaterials*, 2010, **31**, 173–179.
15 R. J. Crawford, H. K. Webb, V. K. Truong, J. Hasan and E. P. Ivanova, *Adv. Colloid Interface Sci.*, 2012, **179–182**, 142–149.
16 F. Gentile, L. Tirinato, E. Battista, F. Causa, C. Liberale, E. M. di Fabrizio and P. Decuzzi, *Biomaterials*, 2010, **31**, 7205–7212.
17 F. Gentile, R. La Rocca, G. Marinaro, A. Nicastri, A. Toma, F. Paonessa, G. Cojoc, C. Liberale, F. Benfenati, E. Di Fabrizio and P. Decuzzi, *ACS Appl. Mater. Interfaces*, 2012, **4**, 2903–2911.
18 A. Allion, J. P. Baron and L. Boulange-Petermann, *Biofouling*, 2006, **22**, 269–278.
19 R. J. Hickey and A. E. Pelling, *Front. Bioeng. Biotechnol.*, 2019, **7**, 1–15.
20 T. P. Kunzler, C. Huwiler, T. Drobek, J. Vörös and N. D. Spencer, *Biomaterials*, 2007, **28**, 5000–5006.
21 P. T. de Oliveira, S. F. Zalzal, M. M. Beloti and A. L. Rosa, *J. Biomed. Mater. Res., Part A*, 2007, **80**, 554–564.
22 N. J. Hallab, K. J. Bundy, K. O'Connor, R. L. Moses and J. J. Jacobs, *Tissue Eng.*, 2001, **7**, 55–70.
23 B. Majhy, R. Iqbal and A. K. Sen, *Sci. Rep.*, 2018, **8**, 1–11.
24 B. Majhy, V. P. Singh and A. K. Sen, *J. Colloid Interface Sci.*, 2020, **565**, 582–591.

25 A. Raj, M. Dixit, M. Doble and A. K. Sen, *Lab Chip*, 2017, **17**, 3704–3716.

26 R. Iqbal, B. Majhy and A. K. Sen, *ACS Appl. Mater. Interfaces*, 2017, **9**, 31170–31180.

27 D. E. Discher, P. Janmey and Y. L. Wang, *Science*, 2005, **310**, 1139–1143.

28 R. G. Wells, *Hepatology*, 2008, **47**, 1394–1400.

29 R. Iqbal, A. Matsumoto, A. Sudeepthi, A. Q. Shen and A. K. Sen, *Appl. Phys. Lett.*, 2019, **114**, 253701.

30 J. Y. Park, S. J. Yoo, E. J. Lee, D. H. Lee, J. Y. Kim and S. H. Lee, *Biochip J.*, 2010, **4**, 230–236.

31 R. N. Palchesko, L. Zhang, Y. Sun and A. W. Feinberg, *PLoS One*, 2012, **7**, e51499.

32 E. Fischer-Friedrich, A. A. Hyman, F. Jülicher, D. J. Müller and J. Helenius, *Sci. Rep.*, 2014, **4**, 4–11.